Journal of Polymer Science

WILEY

JOURNAL OF POLYMER SCIENCE

RESEARCH ARTICLE OPEN ACCESS

Char to the Rescue: Processing and Transfer of Flame-Retardant Epoxy Resins, Adjusting the Fire Behavior and Post-Fire Structural Integrity of Glass Fiber Composites

Sruthi Sunder[1] | Maria Jauregui Rozo[2] | Harshal Deshpande[1] | Alexia Neyer[1] | Vinay Papaiya[1] | Dietmar Meinel[2] | Bernhard Schartel[2] | Holger Ruckdäschel[1]

[1]Department of Polymer Engineering, University of Bayreuth, Bayreuth, Germany | [2]Bundesanstalt für Materialforschung Und -prüfung (BAM), Berlin, Germany

Correspondence: Holger Ruckdäschel (holger.ruckdaeschel@uni-bayreuth.de)

Received: 26 June 2025 | **Revised:** 18 July 2025 | **Accepted:** 21 July 2025

Funding: This work was supported by German Research Foundation (DFG) for funding the project (grant numbers AL 474/53-1 and DFG SCHA 730/26-1).

Keywords: composites | DGEBA | epoxy novolac | post-fire | prepregs

ABSTRACT

Epoxy (EP) glass fiber reinforced composites (GFRCs) are extensively used in structural applications due to their excellent thermal and mechanical properties, but their inherent flammability limits fire-safe deployment. While numerous studies examine the flame retardancy of resins or individual composite systems, comprehensive studies evaluating simultaneous improvements in flame retardancy and post-fire mechanical integrity, specifically through prepreg processing, remain challenging. This study investigates the effectiveness and transferability of phosphorus-based flame retardant (FR) systems to diglycidyl ether of bisphenol A (DGEBA) and EP novolac resin matrices and their corresponding bidirectional glass fiber composites via prepregs. The FRs are chosen based on varying modes of action: ammonium polyphosphate with inorganic silicate (APP/InSi) primarily acts in the condensed phase (CP), and aluminum diethyl phosphinate with zinc hydroxystannate (AldietPO2/ZHS) is known to demonstrate both gas-phase (GP) and CP activity. Fire residues are tailored to compensate for structural defects from fire exposure. EP novolac, with higher aromaticity and cross-linking, possesses better inherent flame resistance compared to DGEBA. The novolac composites containing AldietPO2/ZHS simultaneously showed the highest retention of flexural properties after fire exposure and the best fire safety index. The experimental values of the post-fire flexural properties in the composites calibrated damage parameters in two theoretical models.

1 | Introduction

Epoxy (EP) glass fiber reinforced composites (GFRCs) have widespread application in the automotive, railway, aerospace, and construction industries [1]. This can be attributed to their excellent mechanical, chemical, and thermal properties. However, EP resins possess low inherent flame retardancy. Various strategies for improving the flame retardant properties of EP resins have been extensively studied in the state of the art. These include the use of phosphorus-based flame-retardant (FR) additives that act in the gas phase (GP), condensed phase (CP), or both simultaneously. CP action includes barrier formation via char, intumescence, or glassy or metal oxide residues that reduce heat transfer and fuel release rates [2, 3]. GP action includes the involvement of flame inhibitors and diluents that effectively reduce the spread of the flame [4]. P-based FRs are suitable substitutes for halogenated FRs or others with high loading requirements, such as alumina trihydrate [1, 2]. A combination of ammonium polyphosphate (APP) and inorganic silicate (InSi), in the ratio 8:2, has been reported in literature for its action, primarily in the

CP. This is achieved via char/barrier formation through the intumescent effect of APP in addition to a glass barrier formation via melting and condensation of InSi [5–11]. Another P-based FR found to be effective in EP resins for its combined CP and GP action is aluminum diethyl phosphinate (AldietPO2). Brehme et al. best investigated the different flame retardancy effects of AldietPO2 [12]. AldietPO2 is known for its excellent compatibility with EP resins, specifically diglycidyl ether of bisphenol A (DGEBA) [13]. EP novolac is known to show higher crosslinking ability compared to DGEBA and is inherently more flame retardant than DGEBA due to higher aromaticity [14, 15]. Horrocks et al. reported that AldietPO2 releases $PO^{\bullet}$ and $PO_2^{\bullet}$ in the GP. These less reactive radicals act as flame dilutors in the GP, limiting the concentration of highly reactive radicals involved in flame propagation [16]. The release of such species in the GP causes a simultaneous increase in the release of smoke. This smoke release can be combated using suitable suppressants such as zinc stannate (ZS) or zinc hydroxystannate (ZHS) depending on the temperature stability requirements during processing [16–18]. Additionally, metal phosphates enhance the barrier on the polymer surface and provide flame retardancy action in the CP [16, 19]. Despite established studies for resins, the transfer of these flame-retardant systems to composites via prepregs is challenging due to complex resin-matrix filler interactions. In previous investigations by Sunder and Jauregui Rozo et al. [7–9], it was found that a 10% w/w of APP + InSi was sufficient to confer a UL-94 V-0 rating in a DGEBA resin. However, a 30% w/w loading of the same combination was required to reach the same UL-94 rating in a bidirectional (BD) GFRCs with 55% fiber volume content (FVC). This was attributed to melt flow/wicking effects in addition to the dominance of the glass fibers (GFs) in the overall composite, relaying increased protective layer action but suppressing the other modes of action of the FRs. These findings follow contrasting results by Lim et al. [20] and Rajaei et al. [21] in transferring APP-based FR systems from resins to composites. Thus, the transfer of FRs from resins to composites is not straightforward, and assessing transferability solely based on fire performance indicators in the resins is not sufficient. In addition to the complex interactions involved in flame retardant GFRCs, the post-fire mechanics of such systems are challenging to investigate [3, 22–25]. This is due to the limited range of heat fluxes and time-based test parameters possible for the exposure of EP GFRCs compared to carbon fiber composites [26–28], while maintaining samples still viable for testing. The post-fire mechanical behavior of BD GFRCs containing increasing levels of APP + InSi was investigated on a preliminary basis by Sunder and Jauregui Rozo et al. using a facile sample preparation method [29]. The post-fire mechanical properties of the system were strongly negatively correlated with the increase in char fire residue formation in the systems despite improvements in flame retardancy with increasing levels of APP + InSi. Here, varying fire residues produced by mixed CP and GP action of FRs are considered, with an objective to tailor improvements in both flame retardancy [30] and post-fire mechanics. A systematic investigation is conducted into the transferability of two types of FRs—APP and AldietPO2 with—synergists InSi and ZHS, respectively, which are considered to adjust the flame retardancy and post-fire mechanics. Simultaneously, two different resin systems: DGEBA and EP novolac, and their corresponding composites are used to modify the stability of the fire residue and post-fire mechanics. EP novolac is known to have better inherent flame retardancy and char formation ability [31] which can positively influence post-fire flexural behavior. Thus, the thermomechanical properties of the resins and the composites are compared to understand processing and transfer of FRs to composites using shear viscosity, dynamic scanning calorimetry, and dynamic mechanical thermal analysis. Scanning electron microscopy (SEM) is used for an understanding of the surface morphology of the composites. The pre-fire and post-fire flexural properties via three-point bending testing of the resins and composites containing 30% w/w of the two FR systems are correlated with the respective fire residues obtained from cone calorimeter tests. The ratios of AldietPO2:ZHS and APP:InSi are fixed at 24:6 (8:2) based on past work by the authors [7, 30]. The novelty of this study lies in its comprehensive evaluation of rheological, curing, and microstructure analysis in the transferability of FRs to composites, alongside fire behavior characterization and post-fire mechanical evaluations. Such integrated characterization lays the foundation for deeper insights into resin–filler–fiber interactions, char formation mechanisms, and structural property retention for future optimization and predictive modeling of multifunctional composites tailored for fire-critical applications.

2 | Experimental Section

2.1 | Materials and Methods

2.1.1 | Resin and Composite Formulation and Curing

Table 1 and Table 2 summarize the contents of various resins and the corresponding composites used in this investigation. The ratio of the resin, hardener, and accelerator for the DGEBA:dicyandiamide (DICY):Urone is fixed at a stoichiometric ratio of 100:6.5:1. Further details on the resin dispersion method, resin plate, and prepreg preparation have already been reported previously [8]. The BD GF prepregs, measuring 220 × 300 mm, were subjected to curing in a press setup under a pressure of 50 bar and under vacuum conditions (< 20 mbar). The curing cycles for both the resins and the composites included a starting ramp to 100°C for 2 h, followed by a ramp to 140°C for an additional 2 h and cooldown to room temperature over a minimum of 4 h. The heating rates were constant at ±5°C/min. For the EN systems, the ratio of EN/DICY/UR400 is 100:7.3:1. The curing ramps consisted of a ramp up to 100°C for 1 h. This was accompanied by a ramp to 150°C for 1 h, and another ramp to 170°C for 1 h and cooldown to room temperature over 4 h.

The laminate thickness for all composite formulations was 2.5 ± 0.3 mm when utilizing 5 layers of GFs, and 4.4 ± 0.3 mm with 9 layers of GFs.

2.2 | Processability of the Resins and Composites

2.2.1 | Rheology

The rheological characteristics of the uncured resins were analyzed using an Anton Paar Rheometer (MCR 301). A 1 mm gap was maintained between the parallel plates (PP25). First, a unidirectional temperature sweep measurements over a

TABLE 1 | Summary of FR resin formulations.

	Resins									
	Total active FR %				EN + DICY + UR400	InSi	APP	μAldietPO2	ZHS	
Detailed sample name	P	N	Al	DGEBA DICY + UR400	% wt	% wt of FRs in resin				% wt of GFs
E100	0	0	0	100	0	0	0	0	0	
EN100	0	0	0	0	100	0	0	0	0	
E70InSi6APP24	11.3	3.9	0	70	0	6	24	0	0	0
EN70InSi6APP24	11.3	3.9	0	0	70	6	24	0	0	
E70ZHS6AldietPO2_24	5.14	0	1.7	70	0	0	0	24	6	
EN70ZHS6AldietPO2_24	5.14	0	1.7	0	70	0	0	24	6	

TABLE 2 | Summary of FR composite formulations.

	Composites										
				% wt of resin (incl. FRs) DGEBA system	% wt of resin (incl. FRs) EN system	% wt of FRs in resin				% wt of GFs (DGEBA)	% wt of GFs (EN)
Detailed sample name	P	N	Al								
E100:GF-BD	0	0	0	27	0	0	0	0	0	73	0
EN100:GF-BD	0	0	0	0	25	0	0	0	0	0	75
E70InSi6APP24:GF-BD	2.8	0.8	0	30	0	6	24	0	0	70	0
EN70InSi6APP24:GF-BD	2.8	0.8	0	0	29	6	24	0	0		71
E70ZHS6μAldietPO2_24:GF-BD	1.5	0	0.5	30	0	0	0	24	6	70	0
EN70ZHS6μAldietPO2_24:GF-BD	1.5	0	0.5	0	27	0	0	24	6	0	73

range of 25°C–200°C, at 3 K/min were performed. A 5% shear amplitude with a frequency of 1 rad/s was used. The complex viscosity was checked to ensure a working range between 10 and 50,000 mPa·s based on the recommended limits for the prepreg line [5–9, 32, 33]. Additionally, frequency sweep measurements were performed varying from 0.1 to 100 rad/s with the applied strain constantly maintained at 0.1%, and at a constant temperature of 50°C to ensure linear viscoelastic behavior.

2.2.2 | Differential Scanning Calorimetry (DSC)

The curing process parameters were examined during an initial heating cycle through DSC measurements with a Mettler Toledo DSC 1 (Columbus). A measurement range spanning 25°C–275°C (at 10 K/min) was used. A nitrogen flow rate of 50 mL/min and a sample mass of 5–10 mg were utilized. Per formulation, two samples were tested.

2.2.3 | Dynamic Mechanical Thermal Analysis (DMTA)

Dynamic mechanical thermal analysis (DMTA) was conducted on a Gabo Eplexor 500 N to examine the properties of unreinforced resin, as well as the bidirectional (BD) composite samples. Torsion mode measurements were performed on samples with dimensions of 50 mm × 10 mm × 2 mm. A temperature range of 25°C–180°C (at 3 K/min) was used. The glass transition temperature (T_g) was identified by determining the maximum value of the loss factor (tan δ). Per formulation, two samples were tested.

2.2.4 | Pre- and Post-Fire Flexural Properties

The flexural properties of the resins (pre-fire), and composites (pre- and post-fire) were studied using three-point bending tests (Zwick Roell Z020). The resins and composites tested pre-fire were prepared according to the procedure in 2.1.1. The sample exposure and preparation method for the post-fire flexural analysis of the composites has been described in a previous investigation by Sunder and Jauregui et al. [29]. For the resins, 6–8 specimens with dimensions of 80 mm × 10 mm × 4 mm were tested based on the ISO 178 standard. A crosshead speed of 2 mm/min was maintained. A load cell with a capacity of 20 kN was used. The composite specimens were analyzed based on the EN ISO 14125 norm and measured 100 mm × 15 mm × 4 mm. The load was applied in a transverse direction to the fibers in the 0° direction of the 0°/90° BD composites. In addition to the experimental values of the post fire flexural moduli obtained from the Zwick Roell software (E_F^{post}), the values of the moduli were evaluated

using the secant method and the tangent method. The stress–strain values of the samples exposed at 50 kW/m^2 for 5 min and the resulting flexural modulus were estimated calculating the secant from the linear fit to the data in the strain region 0.1%–0.3% (secant method):

$$E_F^{\text{post\_secant}} = \frac{\sigma_2 - \sigma_1}{\epsilon_2 - \epsilon_1} \tag{1}$$

where σ_1 and σ_2 are the stresses corresponding to strain values ϵ_1 (0.1%) and ϵ_2 (0.3%), respectively. The flexural stiffness from the maximum value of the derivative (tangent method) of the stress–strain curve is calculated as:

$$E_{\text{post}}^{\max} = \left.\frac{d\sigma}{d\epsilon}\right|_{\max} \tag{2}$$

Two theoretical models—the two-layer model proposed by Mouritz et al. [22] and the three-region model proposed by Bibinger et al. [27] were used to compare experimental values of the post fire flexural moduli for all the samples. In the two-layer model, the post-fire flexural modulus E_F^{post2D} is calculated as:

$$E_F^{\text{post2D}} = \left(\frac{4\left(d-d_n\right)^3 + 4\left(d_n-d_c\right)^3}{d^3}\right).E_F^{RT} \tag{3}$$

where E_F^{RT} is the flexural modulus at room temperature, d is the thickness of the sample in mm, d_c refers to the thickness in mm of the char layer, and d_n is the neutral axis of the beam that is calculated by the equation:

$$d_n = \frac{E_F^{RT}d^2 - d_c^2\left(E_F^{RT} - E_c\right)}{2E_F^{RT}d + 2E_cd_c - 2E_F^{RT}d_c} \tag{4}$$

where E_c, is the flexural modulus of the char layer, which is considered negligible and set to 0. The flexural modulus using the three-layer model proposed by Bibinger et al. uses the following equation:

$$\frac{E_{\text{Fres}}^{\text{post\_3}}}{E_F^{RT}} \approx \frac{\sigma_{res}}{\sigma_F^{RT}} = \left(\frac{p_{rIII}}{p_t}.\alpha_{rIII}\right) + \left(\frac{p_{rII}}{p_t}.\alpha_{rII}\right) + \left(\frac{p_{rI}}{p_t}.\alpha_{rI}\right) \tag{5}$$

where $\frac{\sigma_{res}}{\sigma_F^{RT}}$ is the normalized residual strength, p_{rIII}, p_{rII} and p_{rI} are the plies corresponding to regions rIII, rII, and rI, respectively. p_t is the total number of plies, which is 9 in this study. α_{rIII} represents undamaged material contributes fully to the residual strength. α_{rII} is between 0 and 1 and represents partially damaged material which contributes partially to the strength. α_{rI} is 0 and represents severely degraded material which does not contribute to the strength. The number of damaged plies is estimated using grayscale analysis with a threshold of 0.55 on the greyscale set for the damaged areas and a 55% damage percentage set to establish a column in the XCT image as "damaged" (see Supporting Information S1F–G). In the simple model used in the earlier investigation by Sunder et al. [29] the simple three-region model overestimated the contribution of the partially damaged regions and underestimated the proportion of the fully damaged regions resulting in an overestimation of the predicted post fire flexural moduli compared to experimental values. In this study, α_{rII} is therefore calibrated using the advanced three-region model for each sample based on the values between 0 and 1 that give the highest Pearson's correlation coefficient when plotting a linear fit of the experimental and predicted values of the post fire flexural modulus (see Supporting Information S1E, Tables S7 and S8). Using a modified rule of mixture and concepts in the Mori-Tanaka model [34–37] the post fire flexural modulus $E_{\text{post}}^{\text{Mx}}$ is estimated based on the fiber volume fraction in the composites V_f controlled in the prepreg line during manufacture, flexural modulus of the resin matrices at room temperature E_{m0}, and a damage parameter R. R is calibrated based on the maximum value of the Pearson correlation coefficient for a linear fit of $E_{\text{post}}^{\text{Mx}}$ values in the following equation compared to the experimentally measured post fire values E_F^{post}:

$$E_{\text{post}}^{\text{Mx}} = \text{RE}_{\text{m0}}\left[1 + \frac{V_f\left(\frac{E_f}{\text{RE}_{\text{m0}}} - 1\right)}{1 + \left(\frac{E_f}{\text{RE}_{\text{m0}}} - 1\right)\left(\frac{1-V_f}{3}\right)}\right] \tag{6}$$

where E_f is the theoretical flexural modulus of E-glass fibers (70 GPa) and is assumed unmodified after fire exposure.

2.3 | Scanning Electron Microscopy

The composite samples were cut to size (1 mm × 2 mm) and embedded in a cured EP resin (DGEBA). Embedding springs from EpoFix-Struers were used for this purpose. The samples were then analyzed using a scanning electron microscope (Zeiss Gemini 1530-Carl Zeiss AG) at an acceleration voltage of 3 kV. The sample surfaces were sputtered up to a thickness of 5 nm using platinum.

2.3.1 | Cone Calorimetry

All specimens, sized at 100 mm × 4 mm, were assessed in a horizontal orientation under an external heat flux of 50 kWm^{-2} following ISO 5660-1. To avert any interference with the cone heater, the distance between the sample and the heat source was adjusted to 35 mm instead of 25 mm to avoid contact with the cone heater during intumescent growth [38]. The fire safety index (FSI) is expressed as a Petrella plot between the fire load (total heat release or THR) and the fire growth index [39] (FGI) where:

$$\text{FGI} = \frac{\text{pHRR}}{t_{\text{ig}}} \tag{7}$$

where pHRR refers to the peak of heat release rate from cone calorimeter measurements and t_{ig} is the time to ignition.

2.4 | X-Ray Computed Tomography (CT)

A Diondo d2 MAX Cabrio double-tube CT system from Diondo GmbH, Hattingen, Germany, was used for X-ray computed tomography (XCT). A 240 kV microfocus X-ray tube was used as the X-ray source (XWT-240-SE from X-Ray WorX GmbH).

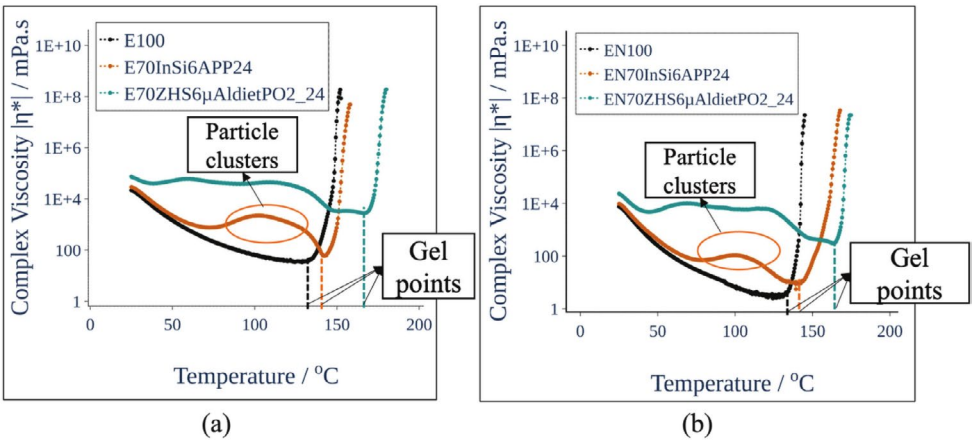

FIGURE 1 | Complex viscosity of the various FR-EP systems (temperature sweep).

The detector used was an amorphous silicon detector panel NDT1717M2/IL with 3000 × 3000 pixels. The CT images were taken in the center part of the approximately 4 mm thick sample after exposure to fire and flexural tests. The set X-ray energy was 80 kV at a current of 250 μA. The image resolution was $(7\,\mu m)^3$ and the images were analyzed using VG Studio MAX software, version 2023.1 (Volume Graphics GmbH).

3 | Results and Discussion

3.1 | Processing and Curing Parameters

3.1.1 | Rheological Properties of the Resins and Composites

The graphs of complex viscosity ($|\eta^*|$) vs. temperature (Figure 1) for E and EN follow similar trends. The viscosity at ~25°C (initial viscosity) measures at ~10,000 mPa·s with a gradual slope downwards due to the increasing mobility of the resin molecules with increasing temperature. At ~140°C for both E100 and EN100, $|\eta^*|$ reaches a minimum value at ~100 mPa·s and 10 mPa·s respectively. $|\eta^*|$ decreases more pronouncedly for EN100 than for E100 due to the increasing significance of shear thinning at elevated temperatures for the branched phenolic backbone compared to the linear flexible DGEBA backbone. Thus, the polymer chains in DGEBA are already mobile, leading to a less dramatic decrease in $|\eta^*|$. Following this, the viscosity rapidly increases indicating cross-linking and cure. In E70InSi6APP24, the curve follows a similar trend to E until ~80°C then slightly increasing and forming a plateau until ~145°C. The plateau observed is attributed to temporary reversible, temperature-dependent microstructural rearrangements between these temperatures. This plateau formation is distinct from the baseline behavior of unfilled systems suggesting transient interactions between particles, potentially via surface-driven clustering or weak agglomeration facilitated by reduced matrix viscosity. These interactions become thermally reversible at higher temperatures, explaining the subsequent decrease in viscosity. This interpretation aligns with prior studies on filled thermoset systems [40, 41], where similar features were linked to temporary increases in filler interactions without permanent agglomerate formation. However, this remains a working hypothesis and will be supported with microstructural validation in future work. Frequency sweep data at 50°C (Figure S1) showed a stable complex viscosity profile over time, indicating that the observed plateau is not due to pre-existing agglomerates, but rather due to thermally induced, reversible microstructural effects such as weak particle-particle clustering. These interactions emerge only as the resin viscosity decreases with heating, and dissipate upon further temperature rise, suggesting a dynamic balance between resin thinning and filler interaction prior to the onset of curing. Subsequently, $|\eta^*|$ of EN70InSi6APP24 decreases, reaching a minimum at ~150°C. The rapid characteristic increase in $|\eta^*|$ is then observed, while slightly slower than the cure reaction compared to E100. For EN70InSi6APP24, a similar plateau is observed, but in a shorter temperature range (~100°C–120°C) and well before the curing reaction takes place at ~150°C. For E70ZHS6AldietPO2_24 and EN70ZHS6AldietPO2_24, the plateau formed by potential particle-particle interactions dominates over a large temperature range between 50°C and 120°C. The stability of the resins at 50°C is confirmed using frequency sweep data (see Figure 1, Supporting Information S1A). The broad plateau in complex viscosity for AldietPO2-containing systems likely arises from transient percolation-like particle networks. The smaller particle size of AldietPO2 (~10 vs. ~20 μm for APP) increases surface contact, promoting particle-particle interactions as resin viscosity drops with temperature. The onset of gelling and cure is delayed until ~170°C for E70ZHS6AldietPO2_24 and ~160°C for EN70ZHS6AldietPO2_24 at the current ramp rate of 3 K/min. The intersection point of G′ and G″ as described in previous work by the authors [7] is used to determine approximate gel points for all the resin formulations which correspond with the onset of cure observed for $|\eta^*|$ versus temperature (see 3.1.2).

The key parameters from the rheology data used for prepreg processing are summarized in the Supporting Information S1B (Table S1). The approximate gel points of the formulations are indicated in the Supporting Information S1C (Table S3).

3.1.2 | Curing Parameters of the Resins and Composites

The first heating cycles of the various resin (Figure 2a,b) and composite formulations (Figure 2c,d) all show decreasing exothermicity of curing reactions (see Supporting Information S1C, Table S3). This phenomenon is especially pronounced in the

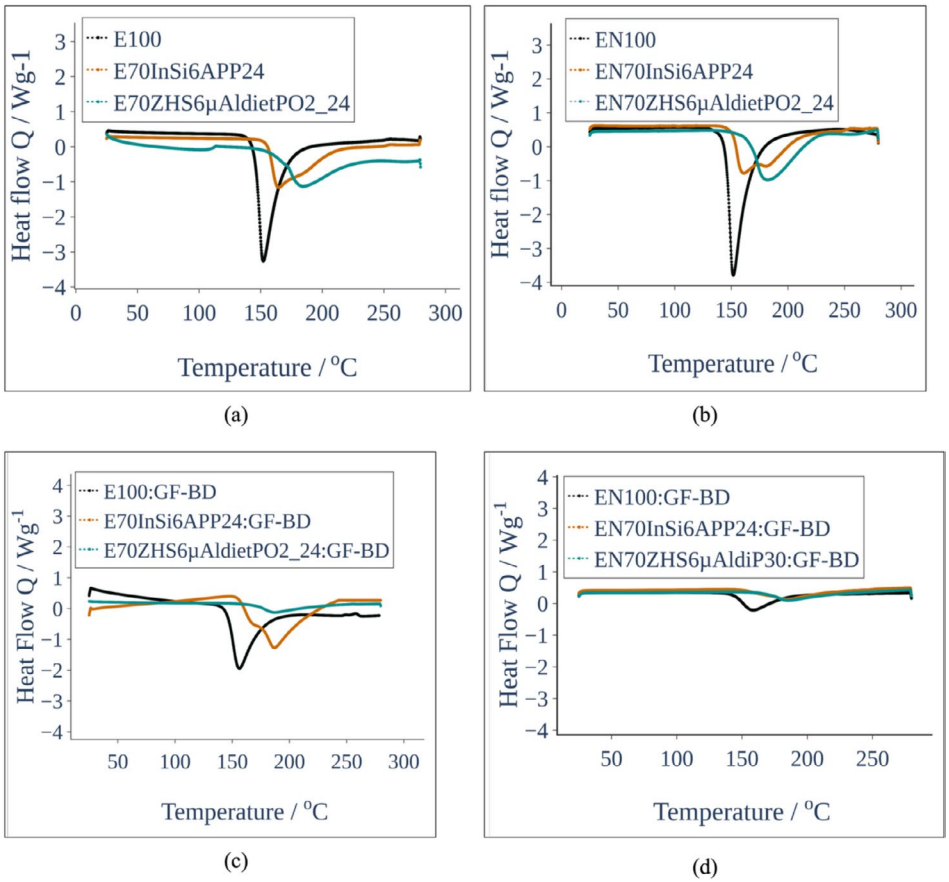

FIGURE 2 | First heating cycles of the various FR systems measured via DSC for resins (a, b) and composites (c, d).

case of the EP novolac composites. In the case of both DGEBA and EP novolac resins the inclusion of the APP/InSi and AldietPO2/ZHS FRs cause a slight shift in the curing peak by ~5°C and ~20°C to higher temperatures, respectively, indicating slower curing at the heating ramp rate of 10 K/min. A similar increase is observed in the EP novolac composites. The APP/InSi-filled systems (E70InSi6APP24, EN70InSi6APP24) display modest shifts in gel point and peak cure temperature relative to their unfilled counterparts, suggesting limited interaction with the curing mechanism [9, 42, 43] at this additive loading and under the tested thermal ramp rate. However, the observed reduction in total curing enthalpy (ΔH ~20%–25%) and slight T_g decrease reflect physical dilution effects, resin-filler interfacial restrictions on mobility, or altered local cure kinetics rather than full chemical inertness. In contrast, the ZHS + AldietPO2 systems (E70ZHS6μAldietPO2_24, EN70ZHS6μAldietPO_24) exhibit more pronounced shifts in curing onset (up to ~25°C) and significantly reduced enthalpies (up to ~135 J/g), alongside notable T_g reductions (ΔT_g ~18°C). These effects suggest a stronger influence on the cure process, which could be due to a combination of reactive interference (e.g., Lewis basicity of phosphinate or ZHS), increased melt viscosity delaying gelation, and potential filler-induced heterogeneity in network formation. Complementary data such as swelling measurements, Soxhlet extraction, or crosslink density estimation, in future studies can determine whether the same crosslink density was achieved or whether the reduced enthalpy reflects an incomplete cure or simply lower heat of reaction per unit resin mass due to dilution. Braun and Schartel reported a mild decomposition effect of AldietPO2 at ~150°C generating phosphinic acid derivatives or aluminum phosphate-like species. These acidic products from AldietPO2 interact with basic ZHS starting at temperatures between 120°C and 150°C as reported by Weil and Levchik et al. [44], Hull et al. [45], and Braun et al. [46] forming insoluble or low-solubility metal-phosphinate salts (zinc phosphinate or tin phosphinates). Such ionic complexes alter epoxy curing kinetics, potentially neutralizing amine groups (hardener) and slowing down the epoxy-amine curing reactions. The effect of these established reactions in the state of the art is considered during the curing cycles of the resins and composites containing AldietPO2/ZHS by increasing the ramp temperatures by 10°C [47] at each stage (see Supporting Information S1C, Table S3). Since the composites contain ~75% % w/w GFs the overall samples have a higher heat capacity, which dampens the temperature rise during the cure reaction leading to less exothermic heat flow peaks observed. Since the GFs are chemically inert, they mildly affect the curing environment at this high proportion (by affecting diffusion of reactive species) thus reducing the observable heat evolution per unit mass. This phenomenon is already reported in literature [48].

3.1.3 | Temperature-Based Mechanics of the Resins and Composites

The tan ∂ peaks of the resins at the T_g are approximately twice that of the composites (Figure 3) indicating a doubling of the loss moduli (G″) of the resins vs. the composites at the same

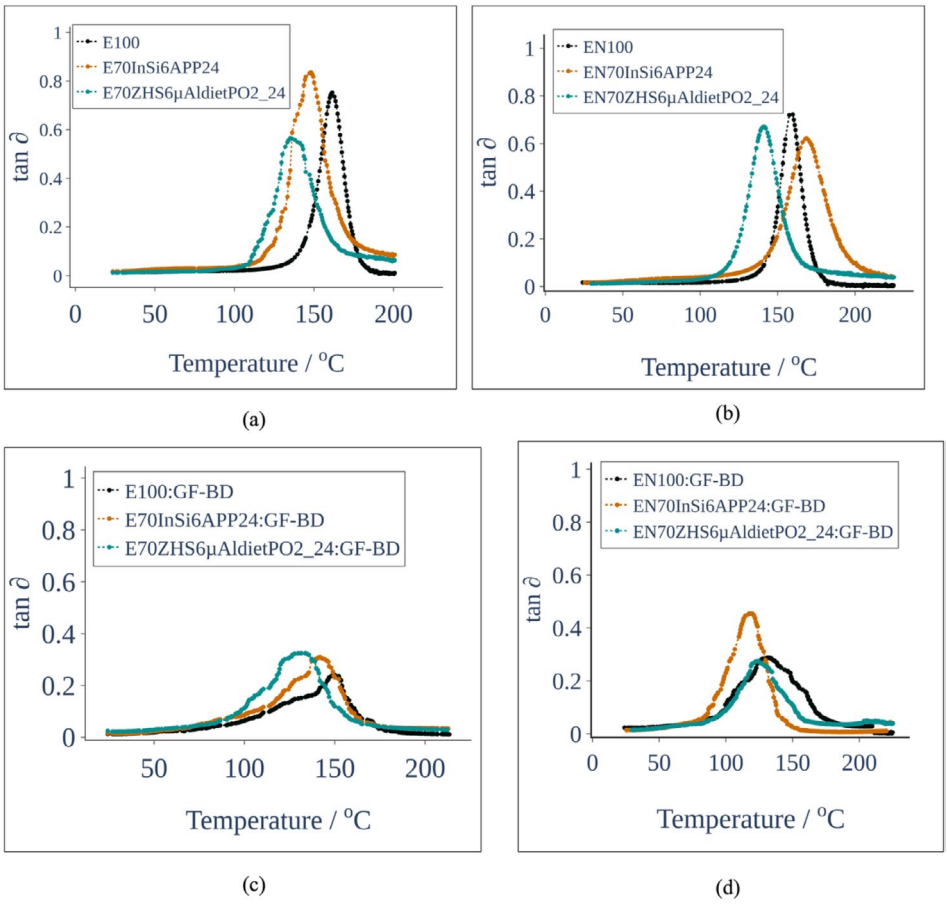

FIGURE 3 | Tan ∂ vs. temperature curves of the resins (a, b) and composites (c, d).

temperature. The T_g of the resins and composites containing APP/InSi vary from the reference systems E100 and EN100 vary negligibly (≤10°C) indicating that APP/InSi interferes less with curing behavior. The resins containing AldietPO2/ZHS show a decrease in T_g of ~18°C for both DGEBA and EP novolac. This corresponds with the observations related to curing enthalpy and peaks in 3.1.2 and the reactions triggered by the initial decomposition of AldietPO2 beginning at ~120°C. This initial decomposition step is integral to AldietPO2 functioning as a flame retardant. The phosphorus-containing species released during decomposition can catalyze char formation or crosslinking at elevated temperatures, thus enhancing char yield and improving thermal insulation properties [46]. With increasing temperature, all storage moduli show a characteristic gentle decreasing slope (Figure 4), followed by a sudden decrease steeply shortly following the T_g. The gentle decline in storage modulus with temperature is due to incremental increases in molecular mobility and free volume. Once the T_g is reached, a rapid change in molecular mobility results in a dramatic loss of stiffness, causing the storage modulus to fall sharply.

The storage modulus does not vary significantly with the inclusion of the FRs between room temperature and ~100°C in both the resins and composites. This is matched by the minor changes to flexural properties at room temperature. The drop in storage modulus occurs sooner for the DGEBA resins and composites containing the AldietPO2/ZHS FR combination, also reflecting the interference with curing onset. AldietPO2/ZHS is more effective in reinforcing the EP novolac system, likely due to the inherent nature of the novolac network and improved interfacial compatibility in the composite. Figure 5 shows a summary of the processing parameters of the resins and composites in this study. The formulations with AldietPO2/ZHS show slightly higher curing onsets and peaks in all DGEBA and EP resins and composites, indicating a slight slowing of the cure reaction which was compensated by increasing the second curing ramp at 140°C–150°C.

3.1.4 | Distribution of Flame Retardants in the Composites

The SEM images (Figure 6) of the cured DGEBA and EP novolac composites are used to understand the FR distribution across the surface of the composites. The FRs were homogenously mixed in the resin using mechanical stirring, and composites are prepared using layers of prepregs impregnated and controlled in-line for resin content. Thus, it is assumed that each layer of the impregnated fibers across the bulk of the composite has a comparable distribution of FRs.

As expected, the reference composite samples show no fillers across both resin and fiber rich areas. For DGEBA with APP/InSi, the distribution of the additives in the resin rich region has been described in detail in previous work and compared to other loading levels by weight of APP/InSi [7]. The distribution

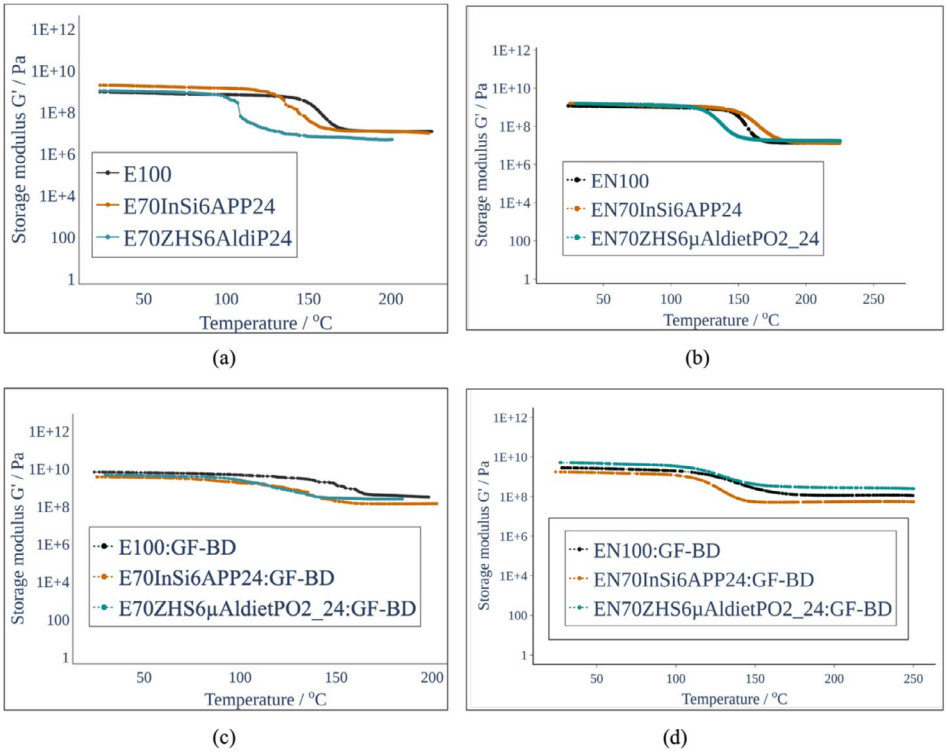

FIGURE 4 | Storage moduli temperature curves of the resins (a, b) and composites (c, d).

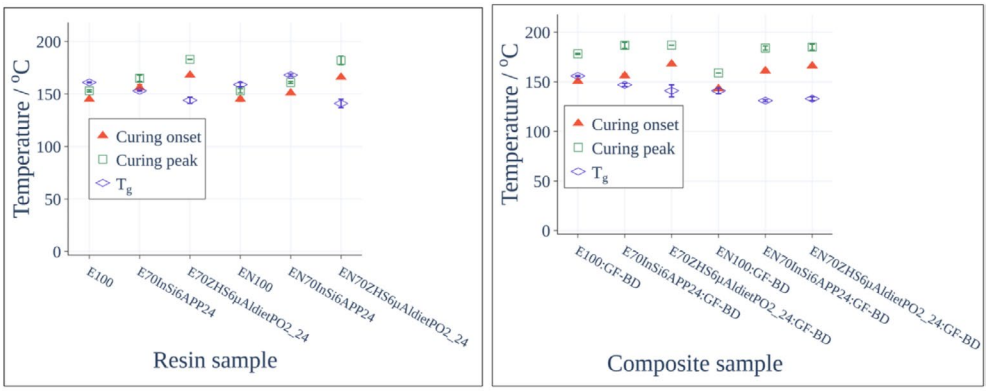

FIGURE 5 | Curing parameters of the resins and BD composites containing different FR compositions.

of the APP/InSi combination in EP novolac is similar, concentrated in the interlayer areas of the composite in between the fibers oriented in 0°/90° directions. Thus, they are likely to act as stress concentrators under mechanical load. In contrast, for the AldietPO2/ZHS combination in both DGEBA and EP novolac composites, the particles are found in the inter-layer regions on the surface of the fibers. Since the particle size of AldietPO2 is ~10 µm and ZHS is ~5 µm, and the pores between the fibers are of a comparable size, the particles are more likely to enter the fiber bundles. The additives form clear clusters at the interface between the resin and the densely packed GFs. AldietPO2 and ZHS have higher affinities toward the polar fiber surfaces (likely sized using organosilanes [49]), increasing the tendency for interface-localization. The concentration of additives near fibers could enhance interfacial bonding, improve fiber–matrix adhesion, and potentially reinforce the composite [50]. In contrast, agglomerations might cause local stress concentrations or weaker resin-rich regions in other parts of the composite [45, 51]. In summary, AldietPO2/ZHS additives localize at the interface between resin and glass fibers with a clear clustering/agglomeration of smaller particles near fiber bundles, resulting in a heterogeneous distribution. The tendency of AldietPO2/ZHS to agglomerate is corroborated by the plateau in the complex viscosity versus temperature data (Figure 1). APP/InSi particles are more evenly dispersed within the inter-layer regions and not strongly accumulated at fiber–matrix interfaces, with fewer agglomerates around the fiber interfaces.

3.1.5 | Fire Safety Index of the Resins and Composites

Figure 7 shows the FSI of the resins and composites with better fire behavior found at the left and lower half of the graph.

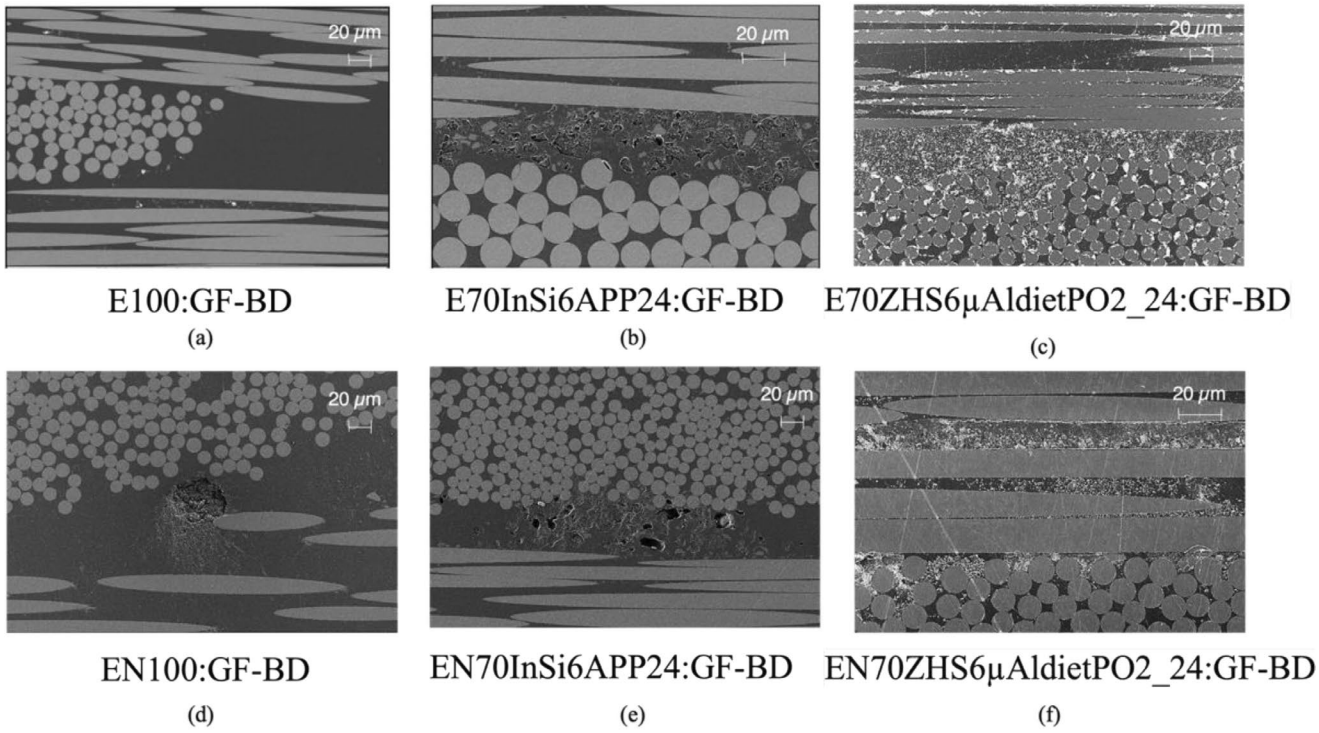

FIGURE 6 | Microstructure of the composites via SEM.

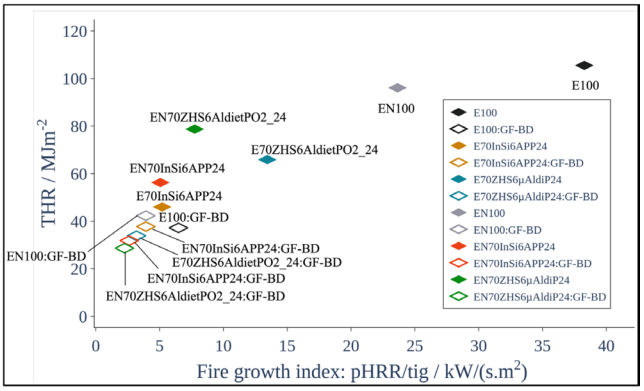

FIGURE 7 | Fire safety indices of the resins and composites.

DGEBA without FRs (E100) is the worst-performing sample with the highest THR and FGI resulting in an FSI of ~38 kWm^{-2} s. In comparison, EP novolac has an improved FSI due to a higher t_{ig} and a lower pHRR (~20%). This is within the range expected, reported by Iji et al. [52] EP novolac resins inherently have higher aromatic content and higher crosslink density, thus creating char more effectively, reducing heat release, and improving thermal stability. With the addition of FRs in DGEBA, the FSI improves further with the samples containing APP/InSi showing the best FGI in DGEBA with an FGI value of ~4 kWm^{-2} s and THR of 33 MJm^{-2} closely followed by the value for EP novolac (FGI~2 kWm^{-2} s, THR~32 MJm^{-2}). Within the composites, EP novolac without FRs (EN100:GF-BD) was the worst performing sample (FGI~4 kWm^{-2} s, THR~42 MJm^{-2}). A detailed investigation of the synergies and other fire performance indices of the DGEBA resins and composites was reported previously [8, 30]. Incorporating synergists like InSi and ZHS was reported to improve flame retardancy, with small variations in pHRR. The presence of the GFs enhanced the fire performance further, reducing HRR, THR, and PHRR and delaying ignition, demonstrating their inert protective effect [30]. The EP novolac composite with AldietPO2/ZHS was found to have the best FSI (FGI~2 kWm^{-2} s, THR~29 MJm^{-2}), compared to existing formulations in previous studies by the authors. A systematic investigation of the potential synergistic effects of AldietPO2 and ZHS in the EP novolac composites will be explored in future. Within the scope of the current study, the concentration of the AldietPO2/ZHS at the fiber interfaces seen in SEM strongly correlates to the improved composite performance in EP novolac systems, potentially reinforcing the char precisely at points in the composite where mechanical and thermal protection is critical. The SEM images showed uniform matrix distribution for APP/InSi rather than at the fiber-interface localization, explaining effective resin char formation but slightly reduced improvement in composite interface stabilization. Although improved flame retardancy is not necessarily an indicator of fire resistance [53] or post-fire mechanics [29], it can be hypothesized that the improved FSI of the EP novolac composites with AldietPO2/ZHS would indicate better post-fire performance than DGEBA composites due to stabilization of the fire residue [54].

Although cone calorimetry tests provide extensive fire performance data, other burning tests such as the UL-94 tests are used to report fire safety in applications such as the electronics industry. UL-94 tests for the DGEBA resins and composites indicated a V-0 rating for all the FR formulations within this study reported elsewhere in detail by Jauregui et al. [30]. A significant improvement in the LOI values compared to the resin without FRs was also evident. Similar tests will be conducted to holistically verify and compare the fire safety of the EP novolac resins and composites further in a future investigation.

3.2 | Pre- and Post-Fire Flexural Behavior

In the DGEBA resin system, introducing the APP/InSi FR causes a slight increase in flexural modulus, while strength and strain both reduce. The inclusion of AldietPO2/ZHS causes a decrease in all three parameters compared to the resin E100 without FRs (Figure 8). The same trend is mirrored in the behavior of the EP novolac resins with both types of FRs. However, the flexural strength and strain of EN100 are higher than those of E100, resulting in a slightly higher modulus. Upon transfer to composites, flexural modulus, strength, and strain reduce with the inclusion of both types of FRs and for both DGEBA and EP novolac composites. The experimental values (Figure 9a) of the post-fire flexural moduli of the composites with DGEBA showed a sharper decrease with the addition of the APP/InSi FRs compared to AldietPO2/ZHS. In contrast, the post-fire flexural moduli of the composites containing both FRs are higher than the reference system EGF100:GF-BD, with the inclusion of the FRs indicating a stabilization of the fire residue. Interestingly, E100:GF-BD shows the highest absolute value of flexural modulus among all the samples. The post-fire flexural moduli evaluated using the two-layer model (Figure 9b) overestimate the value of the moduli by ~50% since it does not differentiate between partially damaged char-containing regions and fully damaged charred regions in the burned composites. A similar result was observed when increasing concentrations of APP/InSi in the BD composite systems were investigated [29]. These discrepancies were also reported by Feih et al. [55] when neglecting gradients in material degradation.

Real damage typically includes partially degraded regions rather than simply undamaged and fully damaged layers. The three-region model and modified rule of mixtures model (Figure 9b) are both equally more effective than the two layer model in predicting the post-fire flexural modulus, based on the calibration of the parameters α_{rII} and the damage coefficient R (see Supporting Information S1E). To adapt the model to the composite-specific char architecture and mechanical degradation, parameters were statistically calibrated to maximize correlation between predicted and experimental values.

Thus, these models can be used as a basis for machine learning predictions and optimization of post-fire flexural parameters using varied resin matrices, FRs, and GF architectures in future investigations using techniques such as Bayesian optimization or active learning [56–58]. The various components within Equations (5) and (6) are promising as input features. Although it appears at the outset as though the inclusion of FRs does not improve the post-fire flexural properties of the composites, the residual flexural strength values (Figure 9c) and moduli (see Table S10) prove otherwise. The EP novolac composites with FRs show the highest residual strengths and moduli (~15% residual modulus/4.6% residual strength for APP/InSi and 16% residual modulus/2% residual strength for AldietPO2/ZHS). This is closely followed by E100:GF-BD (13% residual modulus and

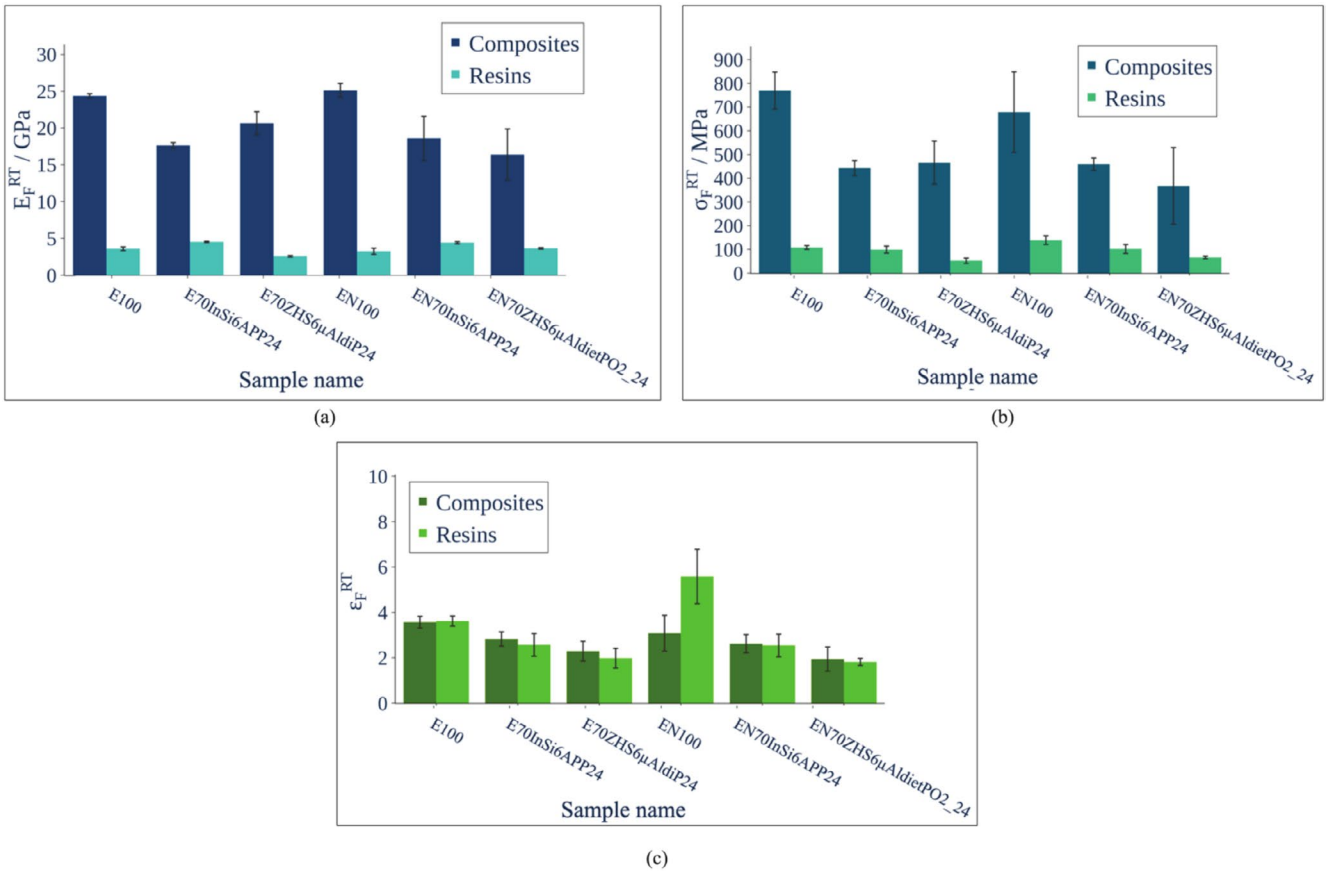

FIGURE 8 | Comparison of the pre-fire flexural moduli (a) strength (b) and strain (c) of the resins and composites.

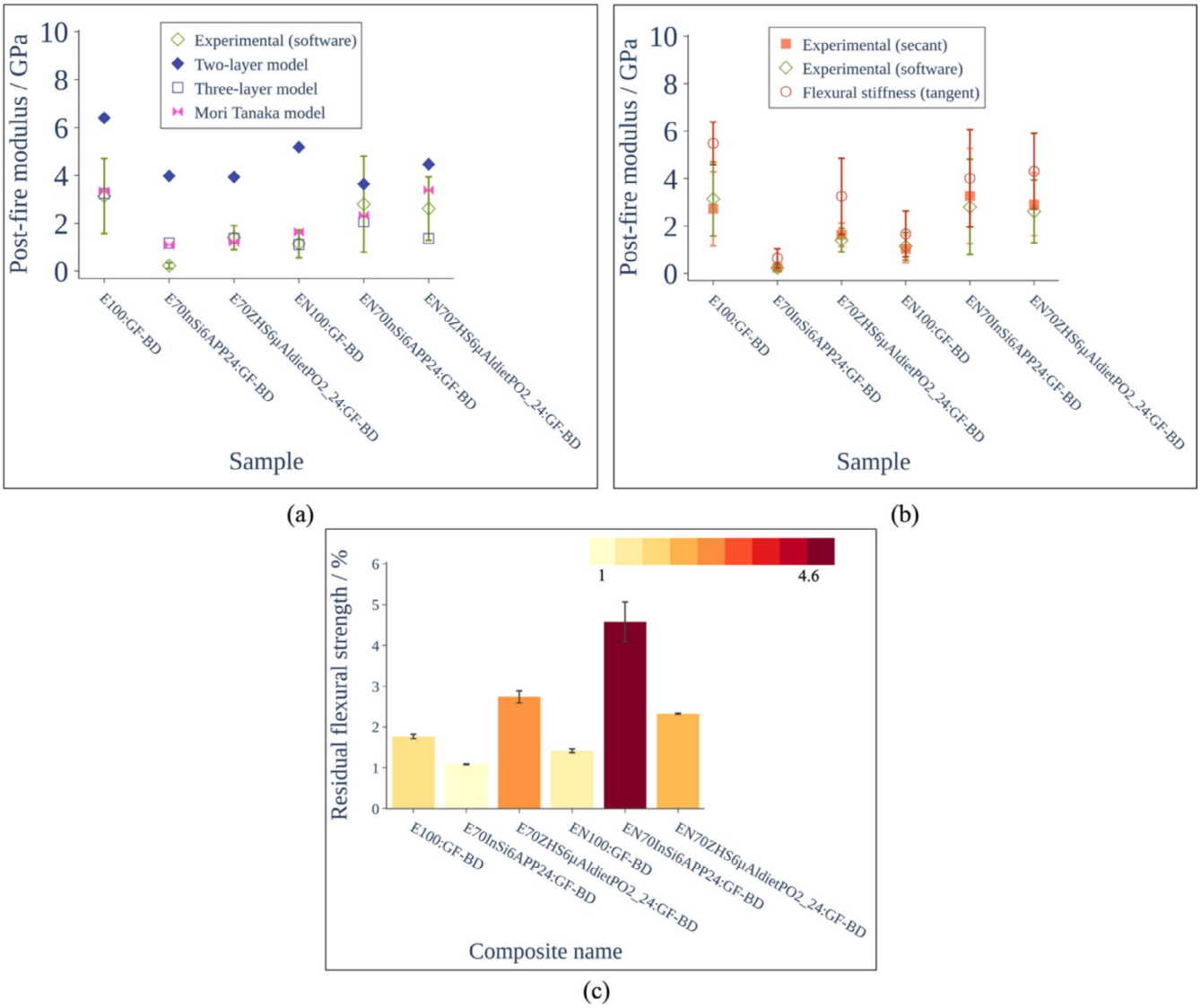

FIGURE 9 | Comparison of the post-fire flexural moduli of the composites based on experimental and theoretical models (a, b) and residual flexural strength (c).

~2% residual strength) and E70ZHS6μAldietPO2_24:GF-BD (6% residual modulus and ~3% residual strength). The DGEBA composite without FRs exhibits the highest initial flexural modulus due to optimal fiber-matrix interactions without FR-induced interference. However, it still performs poorly post-fire due to the absence of protective char, which is shown clearly by significantly lower relative residual modulus and strength. Thus, within the scope of the systems studied here, it appears as though FR additives improve the flame retardancy of the DGEBA composites but not necessarily the post-fire flexural moduli. FRs primarily enhance thermal stability and reduce heat release but introduce internal defects. Using AldietPO2/ZHS at 30% loading with an 8:2 ratio of AldietPO2:ZHS increases the residual flexural strength after fire exposure in both the DGEBA and EP novolac composites compared to the reference systems. Additionally, the inclusion of both the APP/InSi and the AldietPO2/ZHS individual FR combinations in the EP novolac composites improves the flame retardancy, post-fire flexural moduli, and strengths simultaneously. Based on the fire residues in the XCT images (Figure 10) it can be hypothesized that the presence of loose unconsolidated char and structural defects after fire exposure reduces the post-fire residual flexural moduli and strengths of the composites. This is verified by the SEM images of the char microstructure (Figure 11). Example images of the composites and procedure for post-fire testing are shown in Supporting Information S1I.

Comparing the DGEBA and EN composites without FRs, the residues leave the fibers largely unprotected. Addition of the APP/InSi system develops an intumescent, porous char that is more robust in novolac than in DGEBA and emphasized by thicker walls with fewer ruptures. The robust char in the case of the EN composite with APP/InSi explains the higher residual post-fire modulus. Morgan and Gilman et al. implied that intumescent chars from APP are effective thermally but can be mechanically weaker post-fire due to porosity and friability (tendency of the material to crumble under load) [42]. However, in this case, the char is denser but still cracked—suggesting residue yield with limited intumescence. In both DGEBA and EN composites, the AldietPO2/ZHS FR system yields a dense char, especially in the

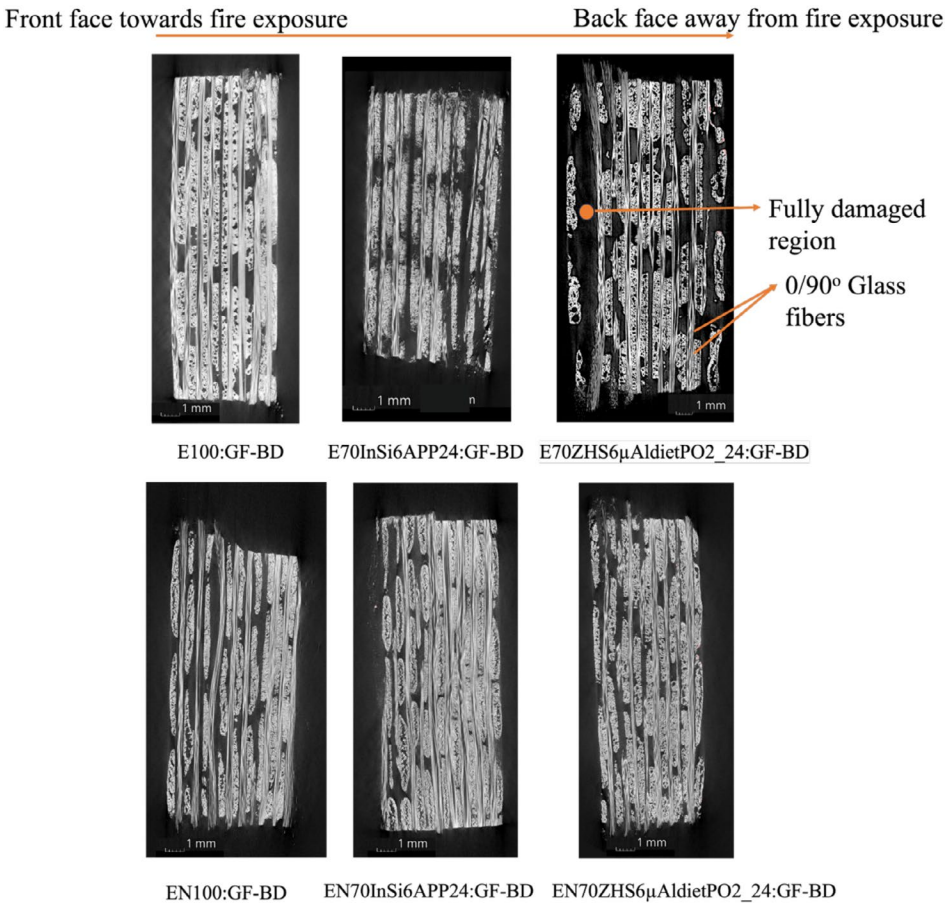

FIGURE 10 | XCT images of the BD composites after fire exposure.

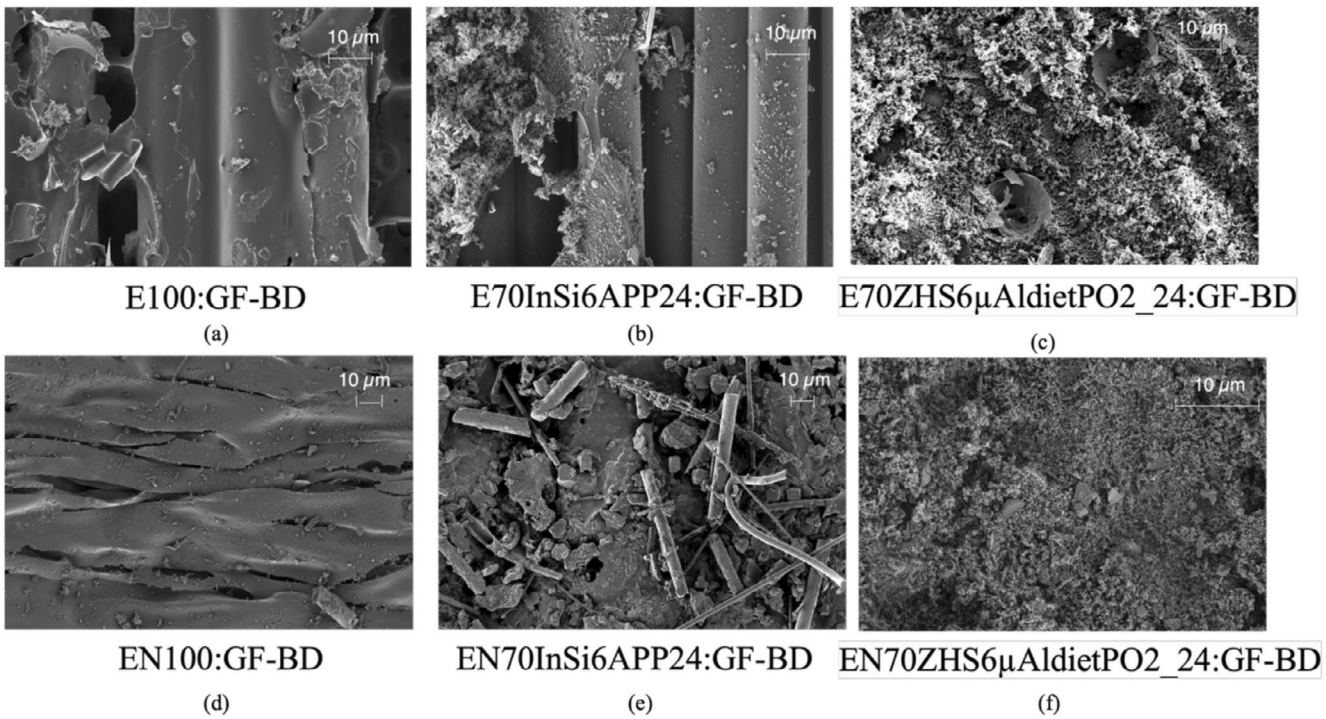

FIGURE 11 | SEM images of the char microstructure post-fire.

novolac system. This corroborates the higher residual post-fire flexural properties for the AldietPO2/ZHS EP novolac composite than the reference without FRs.

4 | Conclusion

In this paper, two different FR systems—APP:InSi and AldietPO2:ZHS in the ratio 24:6 with a total of 30% w/w loading were evaluated in two different EP resin matrices—DGEBA and EP novolac. The two FR systems were chosen based on their established modes of action in the condensed phase (for APP/InSi) and mixed gas/condensed phase action for (AldietPO2/ZHS). The EP novolac matrix was chosen based on its inherently higher flame-retardant capability and higher ability to form a stable char residue than DGEBA. The APP/InSi combination did not interfere significantly with curing behavior in both the DGEBA and EP novolac resins. However, the AldietPO2/ZHS combination displayed effects related to a partial degradation of AldietPO2 at ~120°C leading to a slowdown of the curing reaction due to a reduction in the efficiency of the amine-based curing reaction in both DGEBA and EP novolac resins and composites. The curing cycles of the samples were adjusted by increasing each of the individual ramp temperatures in the curing cycles by 10°C. The presence of the inert GFs dominated the heat flow behavior by acting as heat sinks, thus starkly reducing the curing enthalpy of the composites in comparison to the resins. The APP/InSi FRs were distributed primarily in the resin-rich areas of both the composite surfaces while the AldietPO2/ZHS FRs were agglomerated and distributed closer to the surfaces of the GFs which corresponded with the larger plateau observed in the complex viscosity behavior and their particle sizes. Among the resins, the sample containing APP/InSi showed the best FSI in DGEBA with an FGI value of ~4 kWm^{-2} s and THR of 33 MJm^{-2}. The EP novolac composite with AldietPO2/ZHS was found to have the best FSI (FGI~2 kWm^{-2} s, THR~29 MJm^{-2}). Simultaneously, both the DGEBA and EP novolac composites with the AldietPO2/ZHS combination showed the highest retention of flexural modulus after fire exposure, followed closely by the APP/InSi combination in the EP novolac composite which showed higher retention of both flexural modulus and strength. This was despite the decrease in room temperature flexural properties observed with the inclusion of both types of FRs in both DGEBA and EP novolac composites. Thus, the interactions between matrix-fiber-additive interactions are complex, but adaptable. In future work, the predictive estimation of the post-fire flexural properties of the composites using the parameters relevant to the three-region model and the modified rule of mixtures (Mori-Tanaka) model will be leveraged to build machine learning studies to further optimize post-fire properties.

Acknowledgments

The authors wish to express their gratitude to the German Research Foundation (DFG) for funding the project (grant numbers AL 474/53-1 and DFG SCHA 730/26-1) and Prof. Dr.-Ing. Volker Altstädt for his contribution to the project. The authors thank Alexandra Krasmik for the contribution to preparing the composite structures for post-fire testing. The authors thank Annika Pfaffenberger and Keylab of the Bavarian Polymer Institute (BPI) for their contribution to the SEM measurements. The authors would like to thank Christian Bauer, Ute Kuhn, Andreas Mainz, and Daniel Hohenberger for assistance with sample preparation and testing. The authors also thank Johannes Bibinger for the scientific discussions about the three-region model. Open Access funding enabled and organized by Projekt DEAL.

Conflicts of Interest

The authors declare no conflicts of interest.

Data Availability Statement

The data from this investigation is available from the authors upon reasonable request.

References

1. B. Bilyeu, W. Brostow, and K. P. Menard, "Epoxy Thermosets and Their Applications I: Chemical Structures and Applications," *Journal of Materials Education* 21, no. 5/6 (1999): 281–286.

2. H. Vahabi, M. R. Saeb, and G. Malucelli, *Analysis of Flame Retardancy in Polymer Science* (Elsevier, 2022).

3. B. K. Kandola, F. Magnoni, and J. R. Ebdon, "Flame Retardants for Epoxy Resins: Application-Related Challenges and Solutions," *Journal of Vinyl and Additive Technology* 28, no. 1 (2022): 17–49, https://doi.org/10.1002/vnl.21890.

4. S. Rabe, Y. Chuenban, and B. Schartel, "Exploring the Modes of Action of Phosphorus-Based Flame Retardants in Polymeric Systems," *Materials* 10, no. 5 (2017): 455, https://doi.org/10.3390/ma10050455.

5. W. Liu, Y.-T. Pan, J. Zhang, et al., "Low-Melting Phosphate Glasses as Flame-Retardant Synergists to Epoxy: Barrier Effects vs Flame Retardancy," *Polymer Degradation and Stability* 185 (2021): 109495.

6. G. M. Wu, B. Schartel, M. Kleemeier, and A. Hartwig, "Flammability of Layered Silicate Epoxy Nanocomposites Combined With Low-Melting Inorganic Ceepree Glass," *Polymer Engineering and Science* 52, no. 3 (2012): 507–517, https://doi.org/10.1002/pen.22111.

7. S. Sunder, M. Jauregui Rozo, S. Inasu, B. Schartel, and H. Ruckdäschel, "A Systematic Investigation of the Transfer of Polyphosphate/Inorganic Silicate Flame Retardants From Epoxy Resins to Layered Glass Fiber-Reinforced Composites and Their Post-Furnace Flexural Properties," *Polymer Composites* 45, no. 10 (2024): 9389–9406, https://doi.org/10.1002/pc.28416.

8. S. Sunder, M. Jauregui Rozo, S. Inasu, B. Schartel, and H. Ruckdäschel, "Investigating the Changing Dynamics of Processing, Temperature-Based Mechanics, and Flame Retardancy in the Transfer of Ammonium Polyphosphate/Inorganic Silicate Flame Retardants From Epoxy Resins to Glass Fiber Composites," *Journal of Applied Polymer Science* 141, no. 39 (2024): e55988, https://doi.org/10.1002/app.55988.

9. M. J. Rozo, S. Sunder, H. Ruckdäschel, and B. Schartel, "Char, Gas, and Action: Transfer of the Flame-Retardant Modes of Action in Epoxy Resins and Their Fiber-Reinforced Composites," *Polymer Testing* 140 (2024): 108610, https://doi.org/10.1016/j.polymertesting.2024.108610.

10. S. Wang and R. Ma, "Effect of Phosphorus-Containing Silane Coupling Agents Modified Ammonium Polyphosphate on the Flame Retardancy and Mechanical Properties of Epoxy Resin," *Journal of Applied Polymer Science* 142, no. 17 (2025): e56807, https://doi.org/10.1002/app.56807.

11. R. Ma and S. Wang, "Impact of APP Modified With DOPO Group-Containing Silane Coupling Agent on Flame Retardancy and Mechanical Properties of Epoxy Resin," *Journal of Applied Polymer Science* (2025): e57554, https://doi.org/10.1002/app.57554.

12. S. Brehme, B. Schartel, J. Goebbels, et al., "Phosphorus Polyester Versus Aluminium Phosphinate in Poly (Butylene Terephthalate) (PBT): Flame Retardancy Performance and Mechanisms," *Polymer Degradation and Stability* 96, no. 5 (2011): 875–884.

13. A. Aljamal, G. Marosi, and B. Szolnoki, "Flame Retardancy Effect of Melamine Cyanurate in Combination With Aluminum Diethylphosphinate in a Fully Waterborne Epoxy System," *Phosphorus, Sulfur, and Silicon and the Related Elements* 197, no. 5–6 (2022): 574–578, https://doi.org/10.1080/10426507.2021.2021525.

14. G. Gibson, "Epoxy Resins," in *Brydson's Plastics Materials* (Elsevier, 2017), 773–797.

15. F.-L. Jin, X. Li, and S.-J. Park, "Synthesis and Application of Epoxy Resins: A Review," *Journal of Industrial and Engineering Chemistry* 29 (2015): 1–11.

16. A. R. Horrocks, G. Smart, S. Hörold, W. Wanzke, E. Schlosser, and J. Williams, "The Combined Effects of Zinc Stannate and Aluminium Diethyl Phosphinate on the Burning Behaviour of Glass Fibre-Reinforced, High Temperature Polyamide (HTPA)," *Polymer Degradation and Stability* 104 (2014): 95–103.

17. W. Xu, Z. Zhang, P. Cheng, D. Ding, Z. Bian, and X. Yu, "The Effects of Zinc Hydroxystannate/Boron Nitride Hybrids and Aluminum Diethylphosphinate on Flame Retardancy and Smoke Suppression of Styrene–Butadiene Rubber Composites," *Journal of Applied Polymer Science* 140, no. 44 (2023): e54609, https://doi.org/10.1002/app.54609.

18. L. Zhong, K.-X. Zhang, X. Wang, M.-J. Chen, F. Xin, and Z.-G. Liu, "Synergistic Effects and Flame-Retardant Mechanism of Aluminum Diethyl Phosphinate in Combination With Melamine Polyphosphate and Aluminum Oxide in Epoxy Resin," *Journal of Thermal Analysis and Calorimetry* 134, no. 3 (2018): 1637–1646, https://doi.org/10.1007/s10973-018-7699-4.

19. S. Wang and X. Wang, "Synergistic Flame Retardancy of MIL-88B-Fe Metal–Organic Framework With Aluminum Diethyl Hypophosphite in Epoxy Resin," *Journal of Vinyl and Additive Technology* 31, no. 4 (2025): 824–838, https://doi.org/10.1002/vnl.22210.

20. W. P. Lim, M. Mariatti, W. S. Chow, and K. T. Mar, "Effect of Intumescent Ammonium Polyphosphate (APP) and Melamine Cyanurate (MC) on the Properties of Epoxy/Glass Fiber Composites," *Composites Part B, Engineering* 43, no. 2 (2012): 124–128.

21. M. Rajaei, D.-Y. Wang, and D. Bhattacharyya, "Combined Effects of Ammonium Polyphosphate and Talc on the Fire and Mechanical Properties of Epoxy/Glass Fabric Composites," *Composites Part B: Engineering* 113 (2017): 381–390, https://doi.org/10.1016/j.compositesb.2017.01.039.

22. A. P. Mouritz, "Post-Fire Flexural Properties of Fibre-Reinforced Polyester, Epoxy and Phenolic Composites," *Journal of Materials Science* 37, no. 7 (2002): 1377–1386, https://doi.org/10.1023/A:1014520628915.

23. C. P. Gardiner, Z. Mathys, and A. P. Mouritz, "Post-Fire Structural Properties of Burnt GRP Plates," *Marine Structures* 17, no. 1 (2004): 53–73.

24. N. Kim and D. Bhattacharyya, "Fire Reaction and Post-Fire Impact Properties of Flax Fibre Reinforced Composites Containing Intumescent Flame Retardants," *Journal of Reinforced Plastics and Composites* 43, no. 1–2 (2024): 111–126, https://doi.org/10.1177/07316844231158112.

25. H. Li, E. Kandare, S. Li, et al., "Integrated Thermal, Micro-And Macro-Mechanical Modelling of Post-Fire Flexural Behaviour of Flame-Retarded Glass/Epoxy Composites," *Computational Materials Science* 59 (2012): 22–32.

26. J. Bibinger, S. Eibl, and H.-J. Gudladt, "Influence of Low and Extreme Heat Fluxes on Thermal Degradation of Carbon Fibre-Reinforced Polymers," *Applied Composite Materials* 29, no. 5 (2022): 1817–1840, https://doi.org/10.1007/s10443-022-10043-2.

27. J. Bibinger, S. Eibl, and H.-J. Gudladt, "Ply-Resolved Quantification of Thermal Degradation in Carbon Fibre-Reinforced Polymers," *Journal of Composite Materials* 57, no. 6 (2023): 1057–1072, https://doi.org/10.1177/00219983221150048.

28. T. M. Vetter, J. Bibinger, F. Zimmer, S. Eibl, and H.-J. Gudladt, "Characterization of One-Sided Thermal Damage of Carbon Fiber Reinforced Polymers by Means of Depth Profiles," *Journal of Composite Materials* 54, no. 24 (2020): 3699–3713, https://doi.org/10.1177/0021998320917190.

29. S. Sunder, M. J. Rozo, S. Inasu, D. Meinel, B. Schartel, and H. Ruckdäschel, "Effect of Ammonium Polyphosphate/Silicate Content on the Postfire Mechanics of Epoxy Glass-Fiber Composites Using Facile Chocolate Bar-Inspired Structures," *Fire and Materials* 49, no. 3 (2025): 329–346, https://doi.org/10.1002/fam.3280.

30. M. J. Rozo, S. Sunder, H. Ruckdaeschel, and B. Schartel, "Unveiling Aluminum Diethyl Phosphinate Dual Identity: Transfer From Epoxy Resins to Glass Fiber-Reinforced Composites," *Polymer Composites* (2024), https://doi.org/10.1002/pc.29911.

31. M. R. S. Silveira, V. F. Moritz, C. A. Ferreira, L. Ferry, and J.-M. Lopez-Cuesta, "Flammability of Novolac Epoxy Cured With Aromatic Diamines," *Thermochimica Acta* 741 (2024): 179870, https://doi.org/10.1016/j.tca.2024.179870.

32. M. Demleitner, "Prepreg Technology at Polymer Engineering," n.d., https://www.polymer-engineering.de/wp-content/uploads/2020/12/Prepregs_at_Polymer_Engineering.pdf.

33. C.-H. Ke, J. Li, K.-Y. Fang, et al., "Synergistic Effect Between a Novel Hyperbranched Charring Agent and Ammonium Polyphosphate on the Flame Retardant and Anti-Dripping Properties of Polylactide," *Polymer Degradation and Stability* 95, no. 5 (2010): 763–770, https://doi.org/10.1016/j.polymdegradstab.2010.02.011.

34. C. Wu, Y. Bai, and T. J. Mottram, "Effect of Elevated Temperatures on the Mechanical Performance of Pultruded FRP Joints With a Single Ordinary or Blind Bolt," *Journal of Composites for Construction* 20, no. 2 (2016): 04015045, https://doi.org/10.1061/(ASCE)CC.1943-5614.0000608.

35. T. Mori and K. Tanaka, "Average Stress in Matrix and Average Elastic Energy of Materials With Misfitting Inclusions," *Acta Metallurgica* 21, no. 5 (1973): 571–574.

36. B. Raju, S. R. Hiremath, and D. R. Mahapatra, "A Review of Micromechanics Based Models for Effective Elastic Properties of Reinforced Polymer Matrix Composites," *Composite Structures* 204 (2018): 607–619.

37. B. Gommers, I. Verpoest, and P. Van Houtte, "The Mori–Tanaka Method Applied to Textile Composite Materials," *Acta Materialia* 46, no. 6 (1998): 2223–2235.

38. B. Schartel, M. Bartholmai, and U. Knoll, "Some Comments on the Use of Cone Calorimeter Data," *Polymer Degradation and Stability* 88, no. 3 (2005): 540–547.

39. J. Chen, J. Wang, H. Chen, A. Ni, and A. Ding, "Synergistic Effect of Intumescent Flame Retardant and Attapulgite on Mechanical Properties and Flame Retardancy of Glass Fibre Reinforced Polyethylene Composites," *Composite Structures* 246 (2020): 112404.

40. I. M. Krieger and T. J. Dougherty, "A Mechanism for Non-Newtonian Flow in Suspensions of Rigid Spheres," *Transactions. Society of Rheology* 3, no. 1 (1959): 137–152.

41. C. D. Han, *Rheology and Processing of Polymeric Materials: Volume 1: Polymer Rheology* (Oxford University Press, 2007).

42. A. B. Morgan and J. W. Gilman, "An Overview of Flame Retardancy of Polymeric Materials: Application, Technology, and Future Directions," *Fire and Materials* 37, no. 4 (2013): 259–279, https://doi.org/10.1002/fam.2128.

43. G. Camino and L. Costa, "Performance and Mechanisms of Fire Retardants in Polymers—A Review," *Polymer Degradation and Stability* 20, no. 3–4 (1988): 271–294.

44. E. D. Weil and S. V. Levchik, *Flame Retardants for Plastics and Textiles: Practical Applications* (Carl Hanser Verlag GmbH Co KG, 2015).

45. T. R. Hull, A. Witkowski, and L. Hollingbery, "Fire Retardant Action of Mineral Fillers," *Polymer Degradation and Stability* 96, no. 8 (2011): 1462–1469.

46. U. Braun and B. Schartel, "Flame Retardancy Mechanisms of Aluminium Phosphinate in Combination With Melamine Cyanurate in Glass-Fibre-Reinforced Poly(1,4-Butylene Terephthalate)," *Macromolecular Materials and Engineering* 293, no. 3 (2008): 206–217, https://doi.org/10.1002/mame.200700330.

47. J. M. Barton, "Epoxy Resins and Composites I," *Advances in Polymer Science* 72 (1985): 112–154.

48. B. Wunderlich, *Thermal Analysis of Polymeric Materials* (Springer Science and Business Media, 2005).

49. J. L. Thomason, "Glass Fibre Sizing: A Review," *Composites Part A: Applied Science and Manufacturing* 127 (2019): 105619, https://doi.org/10.1016/j.compositesa.2019.105619.

50. B. Pukánszky, "Interfaces and Interphases in Multicomponent Materials: Past, Present, Future," *European Polymer Journal* 41, no. 4 (2005): 645–662.

51. S. G. Advani and K.-T. Hsiao, *Manufacturing Techniques for Polymer Matrix Composites (PMCs)* (Elsevier, 2012).

52. M. Iji and Y. Kiuchi, "Flame-Retardant Epoxy Resin Compounds Containing Novolac Derivatives With Aromatic Compounds," *Polymers for Advanced Technologies* 12, no. 7 (2001): 393–406, https://doi.org/10.1002/pat.66.

53. M. J. Rozo, S. Sunder, S. Inasu, D. Meinel, H. Ruckdäschel, and B. Schartel, "Weaving Through Fire and Force: Fire Behavior and Fire Stability of Unidirectional, Bidirectional, and Woven Roving Glass-Fiber Composites," *Macromolecular Materials and Engineering* 310 (2025): 2400432, https://doi.org/10.1002/mame.202400432.

54. M. Häublein, K. Peter, G. Bakis, R. Mäkimieni, V. Altstädt, and M. Möller, "Investigation on the Flame Retardant Properties and Fracture Toughness of DOPO and Nano-SiO_2 Modified Epoxy Novolac Resin and Evaluation of Its Combinational Effects," *Materials* 12, no. 9 (2019): 1528.

55. S. Feih, Z. Mathys, A. G. Gibson, and A. P. Mouritz, "Modelling the Compression Strength of Polymer Laminates in Fire," *Composites Part A: Applied Science and Manufacturing* 38, no. 11 (2007): 2354–2365.

56. S. M. Pai, K. A. Shah, S. Sunder, R. Q. Albuquerque, C. Brütting, and H. Ruckdäschel, "Machine Learning Applied to the Design and Optimization of Polymeric Materials: A Review," *Next Materials* 7 (2025): 100449.

57. R. Q. Albuquerque, F. Rothenhäusler, and H. Ruckdäschel, "Designing Formulations of Bio-Based, Multicomponent Epoxy Resin Systems via Machine Learning," *MRS Bulletin* 49 (2023): 59–70, https://doi.org/10.1557/s43577-023-00504-9.

58. S. Meier, R. Q. Albuquerque, M. Demleitner, and H. Ruckdäschel, "Modeling Glass Transition Temperatures of Epoxy Systems: A Machine Learning Study," *Journal of Materials Science* 57, no. 29 (2022): 13991–14002, https://doi.org/10.1007/s10853-022-07372-9.

Supporting Information

Additional supporting information can be found online in the Supporting Information section. **Data S1:** Supporting Information.